Research Article

Nano Biomed Eng

Detection of the Anticancer and Genotoxic Activities of *Heliotropium eichwaldi* L.-fabricated Silver Nanoparticles on BHK-21 Cells and Human Blood Lymphocytes Using MTT and Comet Assays

Naila Sher[1], Mushtaq Ahmed[1]✉, Nadia Mushtaq[2], Rahmat Ali Khan[1]

[1] Department of Biotechnology, University of Science and Technology Bannu-KPK, Pakistan
[2] Department of Botany, University of Science and Technology Bannu-KPK, Pakistan

✉ Corresponding author. E-mail: mushtaq213@yahoo.com

Received: Jul. 11, 2023; **Revised:** Aug. 20, 2023; **Accepted:** Aug. 29, 2023

Citation: N. Sher, M. Ahmed, N. Mushtaq, et al. Detection of the anticancer and genotoxic activities of *heliotropium eichwaldi* l.-fabricated silver nanoparticles on bhk-21 cells and human blood lymphocytes using mtt and comet assays. *Nano Biomedicine and Engineering*, 2023, 15(4): 389−400.
http://doi.org/10.26599/NBE.2023.9290037

Abstract

The possible treatment of cancer with nanoparticles (NPs) would be carried out via inoculation into the veins; as a result, the NPs would come into contact with white blood cells (WBCs) and red blood cells (RBCs) prior to reaching the target cancerous cells. In the current study, the genotoxicity and cytotoxicity potential of silver NPs (AgNPs) against human blood lymphocytes and baby hamster kidney-21 (BHK-21) cells was tested using comet and 3-[4,5-dimethylthiazol-2-yl]-2,5 diphenyl tetrazolium bromide (MTT) assays, respectively. First, AgNPs were created using a *Heliotropium eichwaldi* L. (HE) extract. These AgNPs were then confirmed by ultraviolet–visible (UV–Vis) spectroscopy, which yielded a sharp peak at 416 nm with a maximum absorbance of 1.92. Moreover, an X-ray diffraction (XRD) analysis confirmed the crystalline nature and particle size (19.79 nm) of AgNPs, whereas scanning electron microscopy (SEM) revealed their irregular morphology and size of 30 nm. In turn, an EDX analysis indicated that AgNPs had an appreciable composition of Ag ions (30.68%). According to the comet assay, the HE-AgNPs, and standard H_2O_2 caused highly significant damage to DNA compared with HE extract. The comet assay was reported in terms of the total comet score (TCS). In the case of the MTT assay, a dose-dependent cytotoxicity was noted, in which doxorubicin, and AgNPs were more potent against BHK-21 cells compared with a plant extract. From these results, it is evident that the green-synthesized AgNPs interacted with blood lymphocytes and BHK-21 cells, caused damage to DNA via oxidative stress, and finally triggered cell death (apoptosis). However, further studies aimed at reducing their potential threats are recommended.

Keywords: silver nanoparticles (AgNPs); BHK-21cells; human lymphocytes; comet assay

Introduction

Globally, cancer is the second leading cause of death, after cardiac diseases, as it causes death in the ratio of one in eight individuals, which is greater than that of AIDS, tuberculosis, and malaria [1]. The death ratio caused by cancer worldwide is estimated to rise to 11.5 million in 2030 from the 7.1 million reported in 2002 [2]. Cancer cells divide in an uncontrollable mode because of the loss of signals that keep their division in check, as in normal cells. Cancer has been treated traditionally with chemotherapeutic drugs, and

since the creation of these chemotherapeutic drugs, about five decades have been dedicated to system identification and progress; unfortunately, these chemotherapeutic drugs are associated with various serious life-threatening issues, such as myelotoxicity and cardiotoxicity [3, 4], and were reported to be unsafe [5].

Thus, presently, nanoparticles (NPs) are being used by researchers to diagnose and treat cancer. In this era, nanotechnology plays a crucial role in the consideration, development, and operation of the physicochemical and optoelectronic properties of NPs. Because of the nano size of NPs (1–100 nm), they have gained importance in different fields, i.e., imaging, cosmetics, anticancer, antioxidant, sensor, and drug-carrier agents [6].

Human exposure to NPs is inevitable, as they are being widely used; therefore, emerging toxicity issues are now attracting attention. For biomedical purposes, especially *in vivo* applications, toxicity is a critical factor to consider when evaluating the potential of NPs. Exposure to certain cytotoxic agents can disturb the cell membrane, which allows the cellular contents to leak out or affects mitochondrial activity [7]. It has also been claimed that the induction of reactive oxygen species (ROS) is a general mechanism of NP-mediated cytotoxicity. *In vitro* exposure to AgNPs causes a reduction in the level of glutathione (GSH), an increase in ROS levels, lipid peroxidation, and increased expression of ROS-responsive genes. In turn, an increase in ROS levels was reported to be associated with DNA damage, apoptosis, and necrosis [8]. Interestingly, AgNPs exhibit anticancer properties against various cancer cell lines, such as MCF-7 breast cancer cells [9, 10], HCT116 colon cancer cells, prostate cancer cells [11], HeLa cells [12], and lung carcinoma A549 cells [13].

Different types of NPs have been reported, such as Au, Zn, Cu, Ag, and Fe NPs; however, among these metal-based NPs, AgNPs are appreciable traditionally because of their low toxicity, cost-effectiveness, and health-preserving nature. According to the literature, AgNPs possess a potential as anticancer agents and can be used as a green nontoxic treatment to replace chemotherapy [14]. AgNPs also hold a potential for genotoxicity, which is characterized by the breakage of double-stranded DNA (dsDNA) and chromosomal instability, finally leading to cell death via apoptosis [15–17]. The comet assay is an inexpensive and quick process that is most commonly used for determining DNA damage in terms of the total comet score (TCS) [18].

AgNPs are synthesized via both chemical and biological methods; however, because of the use of toxic, expensive, and environmentally unfavorable reagents, the chemical method is not favored for the synthesis of AgNPs. Thus, researchers have favored biological methods for AgNP synthesis, especially herbal synthesis of AgNPs using plant extracts as reducing, capping, and stabilizing agents. Thus, green synthesis has emerged as an efficient field of nanotechnology. Globally, the herbal synthesis of AgNPs has gained much importance because of its low cost, nontoxic nature, simplicity, and environmentally favorable process [19].

Heliotropium eichwaldi L. (HE), which is a species in the family Boraginaceae, is commonly known as uthchara. People have long utilized this herb to heal a variety of ailments; e.g., to treat earache, the leaves are folded up and placed into the ear. It additionally serves to treat migraine and ulcers [20, 21]. Thus, given the importance of green-fabricated AgNPs, the current study was designed to synthesize HE-AgNPs. The resulting AgNPs were then characterized using several important techniques, such as ultraviolet–visible (UV–Vis) spectroscopy, X-ray diffraction (XRD), scanning electron microscopy (SEM), Fourier transform infrared spectroscopy (FTIR), and energy dispersive X-ray spectroscopy (EDX). Furthermore, their genotoxicity was assessed via comet and 3-4.5-dimethylthiazol-2-yl)-2,5-diphenyltetrazolium bromide (MTT) assays, to test their anticancer activity in baby hamster kidney-21 (BHK-21) cell cultures via apoptosis.

Experiments

Materials

Silver nitrate salt ($AgNO_3$) was obtained from Sigma (USA). BHK-21 cells maintained in Glasgow Minimum Essential Medium (GMEM) were obtained from Foot and Mouth Disease Vaccine Research Center, Veterinary Research Institute, Peshawar (FMDRC-VRIPeshawar). The 3-4.5-dimethylthiazol-2-yl)-2,5-diphenyltetrazolium bromide (MTT), andpenicillin-streptomycin were bought from Sigma-Aldrich, trypsin was obtained from LonzaChemicals, Nansha, China. Doxorubicin HC1 (10 mg) from A1 Habib pharmaceuticals. The reagents used in the

comet assay technique were phosphate-buffered saline (PBS), 1% normal melting agarose (NMA), 1% low melting point agarose (LMPA), lysing solution (100 mmol/L ethylenediaminetetraacetic acid (EDTA), 2.5 mol/L NaCl, 10 mmol/L Trizma base, 1% Triton X-100, and 10% dimethyl sulfoxide (DMSO)), electrophoresis buffer (300 mmol/L NaOH and 1 mmol/L sodium ethylenediaminetetraacetic acid (EDTA), pH 13), neutralization buffer (0.4 mol/L and dHO), andstaining solution (acridine orange 20 μg/mL). All other reagents used were of analytical grade.

Plant gathering and extract preparation

Dr. Tahir Iqbal of the University of Science and Technology in Bannu identified the HE plant with voucher No. NS1. The plant was subsequently dried out, crushed, and extracted with 70% methanol in a w/v ratio of 1:3. After 7 days of soaking in methanol, it was filtered, and the filtrate was evaporated to a crude extract, which was for further experimentation [22].

Synthesis of AgNPs

The protocol reported in Ref. [23] was used for AgNP synthesis. An $AgNO_3$ solution (1 mmol/L in deionize water (diH_2O)) with optimum pH (0.1 mol/L HCl and NaOH were used to alter the pH) was prepared. The HE extract (1 mg/100 mL diH_2O) was centrifuged for 30 min at 6 000 r/min and the supernatant was collected. This plant supernatant and the 1 mmol/L $AgNO_3$ solution (pH 11) were mixed at a ratio of 1:1. A yellowish-brown color was observed after 3 h of mixing the solutions at 40 ºC. This coloration indicated the reduction of the Ag ions. For the complete reduction of Ag and the generation of stable AgNPs, the solution was incubated for 24 h. A UV spectrum analysis was then performed to confirm the peak and concentration of AgNPs in aqueous solution. At −4 °C, the aqueous solution was centrifuged for 10 min (10 000 r/min) to recover the pellet, which was further lyophilized to a powder form. These powdered AgNPs were then used for characterization and the determination of their biological activities, as shown in Fig. 1.

Characterization

A Shimadzu UV spectrophotometer (UV-1800), a Shimadzu Corporation (IR Prestige-21) spectrometer (Japan), a Jeol-jdx-3532 (Jeol Japan) X-ray diffractometer, a scanning electron microscope (model JSM-5910; Japan), and a Jeol J5-M-IT-100

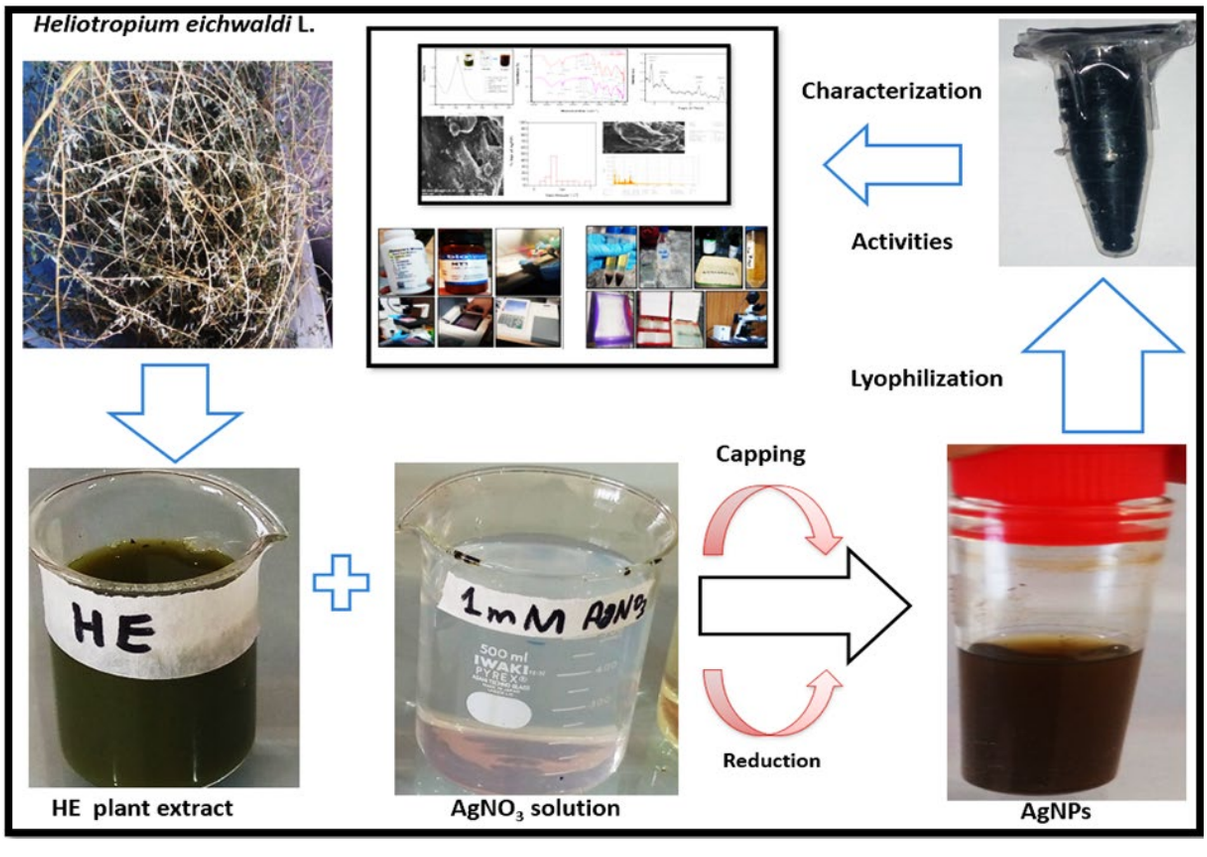

Fig. 1 Stepwise process of the HE-based fabrication of AgNPs.

electron diffraction X-ray spectroscope were employed for analyzing the AgNPs, to confirm their concentration, surface-coating reagents, crystalline nature, surface morphology, and elemental composition, respectively.

Alkaline comet/genotoxicity assay

A modified procedure of the protocol reported in Ref. [24] was used to perform the genotoxicity assay. Briefly, 3 mL of blood was collected from normal human individuals (male of female) into K-EDTA disposable labeled tubes and stored in a freezer. The blood samples were centrifuged via Histopaque-1077 density gradient to obtain lymphocytes. PBS was added to the blood, followed by centrifugation at 3 000 r/min for about 30 min. After centrifugation, the middle buffy layer (lymphocytes) was carefully collected and centrifuged at 3 000 r/min for 5 min. The pellet was mixed with 500 μL of PBS, and 50 μL of lymphocytes was taken from this solution and mixed with 50 μL of samples at different concentrations (25–600 μg/mL), then incubated at 37 °C for 3 h. This experiment was performed in triplicate. Precoated slides were prepared by placing the slides in 0.7% NMA, followed by drying; subsequently, the agarose under the slides was removed and they were incubated for 24 h at 20–25 °C. Then, 75 μL of 0.7% LMPA and 10 μL of the mixed lymphocyte and sample mixture were combined and dispersed on the previously coated slides. A cover slip (22 mm × 22 mm) was held in place for 5 min at 0 °C. The cover slip was removed and 85 μL of LMPA was added to the slide, which was then topped with a cover slip. The cover slip was removed again after 5 min of incubation at 0°C. The slides were then maintained in cooled reducing solution (0.01 mol/L Tris, 0.1 mol/L Na_2EDTA, 1% Triton X-100, 2.5 mol/L NaCl, 10% DMSO, pH 10) overnight at 4 °C. The slides were rinsed with Milli-Q water after lysing, and then stored in cooled electrophoresis solution (0.001 mol/L EDTA, 0.3 mol/L NaOH, pH 13). To unwind and precise the DNA and break the dsDNA and ssDNA, the slides were placed in electrophoresis buffer for 20 min. Gel separation was performed at 300 mA and 25 V for 25 min. The slides were rinsed with a neutralized buffer after phoresis (pH 7.5, 0.4 mol/L Tris), then treated with ethanol for fixation and stained with the chromogenic acridine orange dye (20 μg/mL). The slides were examined using a fluorescence microscope (Nikon Eclipse 80i) with an excitation filter of 450−490 nm. One hundred cells were selected per slide visually and classified into five groups, i.e., class 0 corresponded to absence of DNA damage, and class 4 corresponded to the highest DNA damage [25]. For total comet score (TCS) calculation, the following formula was used [26],

$$\mathrm{TCS} = 0(N) + 1(N) + 2(N) + 3(N) + 4(N)$$

where N is the total quantity of cells in each of the classes.

Anticancer assay

Ethical approval

The anticancer activity of the AgNPs was assessed *in vitro*; therefore, ethical approval was not required.

Study zone

The anticancer activity was assessed at FMDRC-VRI Peshawar, Pakistan.

Assessment of anticancer activity using the MTT method

The cytotoxic activity of the AgNPs against BHK-21 cells was analyzed using the following protocol [27]. GMEM was used for BHK-21 cell culturing; 100 mL of the medium used for cell growth contained 89 mL of GMEM (12.52 g/L in H_2O), 1 ml of antibiotics (penicillin–streptomycin), 10 mL of serum, and 0.4 g/L $NaHCO_3$ (for maintaining the pH at 7.2–7.4). For 2 days, a cultivation beaker (75-cm^2 cell) was incubated at 37 °C. The medium was replaced with fresh medium 24 h later. After 2 days of culture, the cells were placed in 96-well plates. For detaching the cells from the walls, the cells were treated with 2 mL of trypsin. Each well received 100 μL of BHK-21 cells (1×10^5 cells/mL) and was incubated for 1 day at 37 °C. The medium was removed after incubation, and 100 μL of 4% serum was added to each well. Subsequently, the cells were treated with 100 μL of each sample (25–600 μg/mL) and incubated for 2 days at 37 °C. Doxorubicin was used as a standard. The cultured cells received treatment with 100 μL of yellow MTT solution (0.5 mg/mL GMEM) 2 days later and were incubated for 4 h at 37 °C. Next, 100 μL of DMSO was added to each well. The entire experiment was carried out in a Class II A-2 Biosafety Cabinet. The plate was shaken at 150 r/min for 5 min, and the purple formazan solution was examined at 450 nm on an ELISA reader (AMP Platos R II Microplate Reader). Cell viability was determined using the following equation,

$$\text{Cell viability } (\%) = \frac{\text{Sample OD}}{\text{Control OD}} * 100$$

Statistical analysis

For the statistical analysis, one-way analysis of variance (ANOVA) followed by a post-hoc analysis (Duncan multiple range tests) was used. The coefficient of correlation was determined using Statistics (version 8.1 USA). Graphs were plotted in SlideWrite and Origin. Significance was set at $P < 0.05$.

Results

UV–Vis analysis

Ag ions that were optically converted to stable AgNPs were reported in the current study after combining the plant material with the $AgNO_3$ solution. The range of the spectrophotometer was set between 200 and 800 nm. The aqueous extract of the HE plant exhibited no absorption peak in the set range, whereas AgNPs gave a sharp peak at 416 nm, which confirmed the formation of AgNPs after 24 h of incubation at 40 °C (Fig. 2).

FTIR analysis

The FTIR analysis of both samples, i.e., HE plant extract, and HE-AgNPs, showed various peaks that corresponded to specific functional groups of the phytochemicals (Fig. 3). The characteristic peaks were reported in the range of 3 400–600 cm^{-1}, which showed the different metabolites in the HE extract and HE-AgNPs (Table 1).

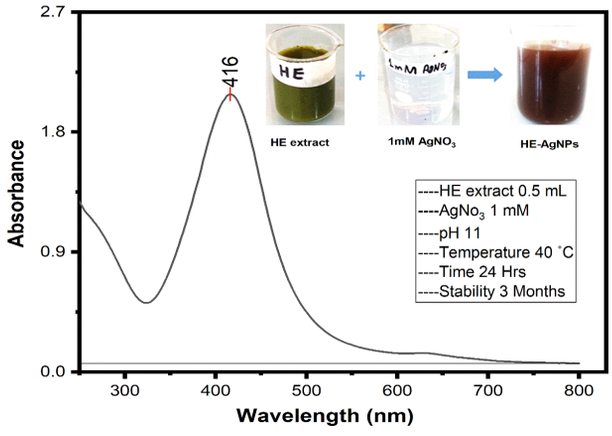

Fig. 2 UV–Vis spectrum of the AgNPs.

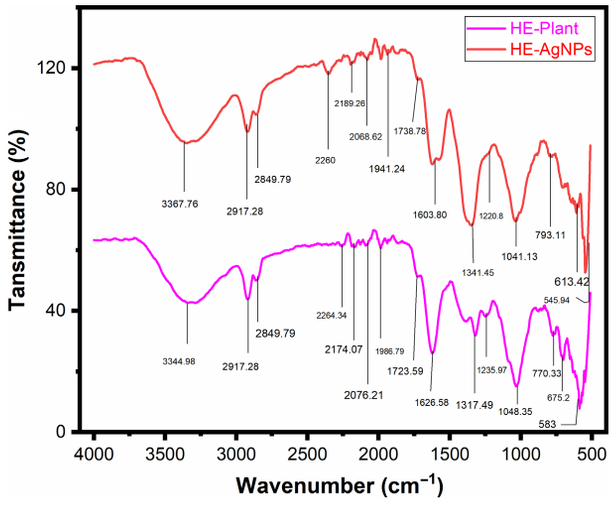

Fig. 3 Plant extract and AgNP analysis using FTIR.

Table 1 FTIR analysis of the HE extract and AgNPs

S. no	Wavelength (cm^{-1})	Wavelength of HE-plant (cm^{-1})	Wavelength of AgNPs (cm^{-1})	Functional group assignment	Phyto compounds identified
1	3 570–3 200	3 344.98	3 367.76	O-H stretch, Hydroxy group, H-bonded	Poly hydroxy compound
2	2 935–2 915	2 917.28	2 917.28	Asymmetric stretching of –CH (CH_2) vibration,	Lipids, protein
3	2 865–2 845	2 849.79	2 849.79	Symmetric stretching of –CH (CH_2) vibration,	Lipids, protein
4	2 260–2 100	2 264.34	2 260	C≡C stretchCarbon–Carbon triple bond	Terminal alkynes
5	2 100–1 800	1 986.79	1 941.24	Carbonyl compound frequency	Transition metal carbonyls
6	1 700–1 725	1 723.59	1 738.78	C=O stretch, Carbonyl	Carbonyl compound
7	1 650–1 600	1 626.58	1 603.80	C=O stretching vibration, Ketone group	Ketone compound
8	1 410–1 310	1 317.49	1 041.13	O–H bend, Alcoholic group	Phenol or tertiary alcohol
9	1 325–1 215	1 235.97	1 220.8	C–H stretch	Alkyl ketones
10	1 100–1 000	1 048.35	1 041.13	Phosphate ion	Phosphate compound
11	800–700	700.33	793.11	C–Cl stretch	Aliphatic chloro compound
12	700–600	675.2	613.42	C–Br stretch	Aliphatic bromo compounds
13	690–550	583	545.94	Halogen compounds (bromo compounds)	Aliphatic bromo compounds

XRD analysis

The crystal structure of the AgNPs was determined by XRD in the current work. Four Bragg reflections at various angles of 38.41°, 44.48°, 64.56°, and 77.47° are indicated in Fig. 4, which were linked with (1 1 1), (2 0 0), (2 2 0), and (3 1 1) planes, respectively. These peaks validated the crystalline structure of the AgNPs. The Debye–Sherrer equations (1), (2), and (3) were used to calculate the size (D), interplanar space (d), and Miller coefficients (a^o), respectively. A mean size of 19.79 nm was reported for all 4 peaks (Table 2).

$$D = k\lambda/(\beta\cos\theta) \quad (1)$$

$$d_{hkl} = \pi/2\sin\theta_{hkl} \quad (2)$$

$$\alpha^o = d_{hkl}(h^2 + k^2 + l^2)^{1/2} \quad (3)$$

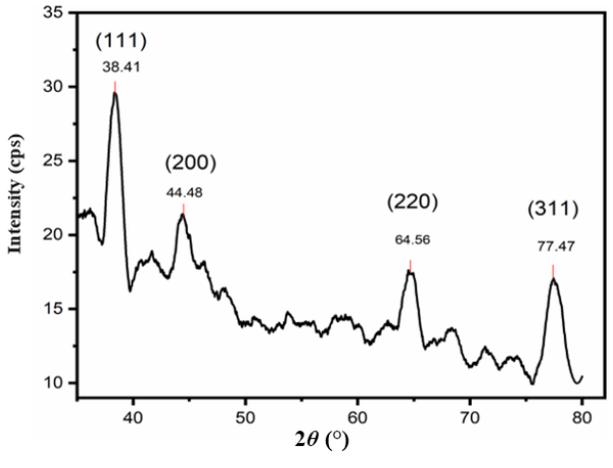

Fig. 4 AgNPs XRD pattern evaluation.

EDX analysis

Figure 5 shows the validation of the composition of the elements of the AgNPs by EDX analysis. The Ag composition of the AgNPs was reported to be 30.68%, whereas the remaining surface-coated elements were reported to be C at 28.72% and O at 40.60%; thus, the EDX analysis provided complete information about the purity of the AgNPs.

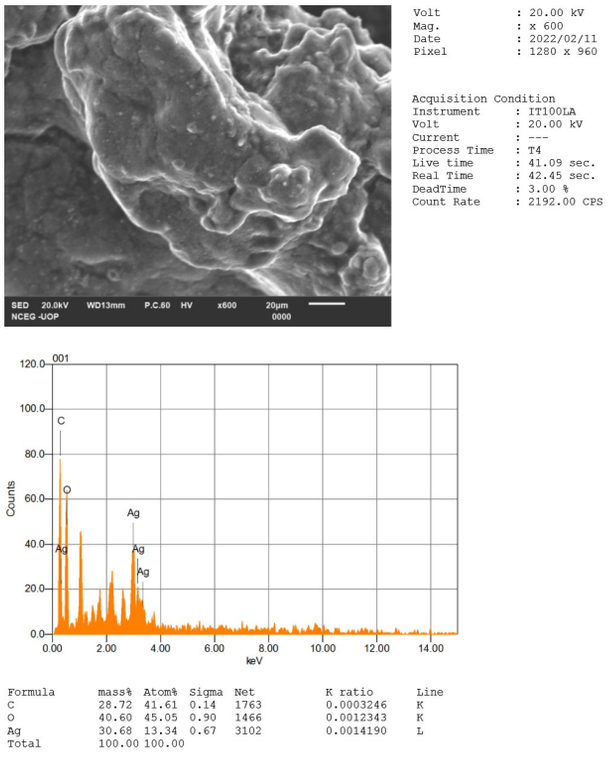

Fig. 5 EDX-based evaluation of the AgNPs. Ag confirmed the existence of AgNPs.

SEM analysis

The SEM image revealed irregularly shaped AgNPs with a size of 30 nm, which was calculated using a nano measuring software (with a range of 1 µm) by marking 15 particles in the SEM image. It is also reported that 48.24% of the AgNPs had a size of 30 nm (Fig. 6).

Genotoxicity (comet assay)

The comet assay revealed that the AgNPs caused DNA strand breaks in human blood cells in a concentration-dependent manner and exhibited higher genotoxicity compared with the plant extract, whereas they exhibited low comet formation compared with H_2O_2 (as a positive control). DNA damage was measured as TSC and was reported to be 197.6 ± 1.5 for HE, 207.3 ± 2.5 for AgNPs, 240 ± 7.2 for H_2O_2 (at 600 µg/mL), and 96.6 ± 3.1 for the negative control (Table 3). Almost no comet tails were observed in the

Table 2 Determination of the interplanar spacing and lattice constant of AgNPs.

S. No	2θ value	Element	*hkl*	FWHM (β) of intense peak (radian)	Particle size (nm)	Interplanar spacing (d)	Lattice constants (a_0)
1	38.41°	Ag	1 1 1	0.0069	20.08	2.34 Å	4.05 Å
2	44.48°	Ag	2 0 0	0.00436	31.78	2.03 Å	4.06 Å
3	64.56°	Ag	2 2 0	0.013	18.92	1.44 Å	4.07 Å
4	77.47°	Ag	3 1 1	0.0165	8.40	1.23 Å	4.04 Å

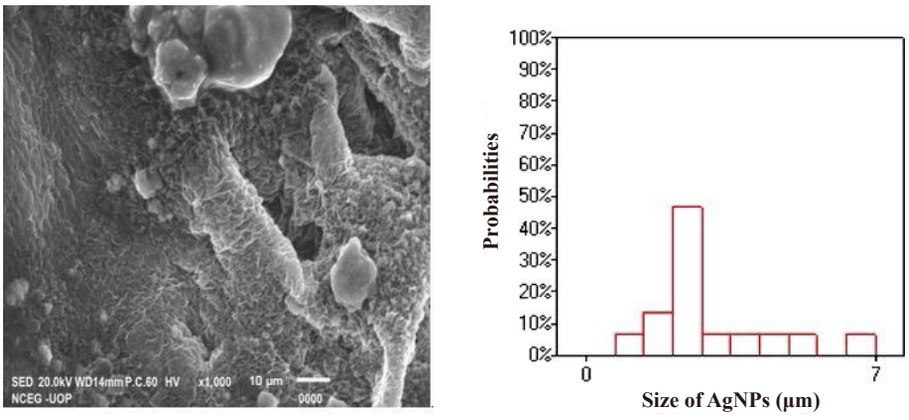

Fig. 6 SEM images of the AgNPs. The white spots represent AgNPs.

Table 3 Effect of the HE plant extract, AgNPs, and H_2O_2 on lymphocytes.

HE-plant ex						
Comet class	25 µg/mL	50 µg/mL	100 µg/mL	200 µg/mL	400 µg/mL	600 µg/ml
0	43.3 ± 10	29.3 ± 1.5	26 ± 1	22.6 ± 2.1	22.3 ± 1.5	18 ± 1
1	2.6 ± 3	25.6 ± 0.57	23.6 ± 0.57	21.6 ± 2.1	21 ± 1	21.3 ± 0.6
2	16 ± 2	21 ± 1	21 ± 1	21.6 ± 1.5	20 ± 2	23.3 ± 0.6
3	11 ± 4.5	15 ± 1	18.6 ± 2.1	22 ± 5	23 ± 5.2	119.6 ± 0.6
4	8 ± 4	9 ± 2	10.6 ± 3	12 ± 3	13.6 ± 1.5	17.6 ± 0.6
TCS	117.3 ± 31	150 ± 10	172.6 ± 20	179 ± 10	184.6 ± 6.5	197.6 ± 1.5
AgNPs						
Comet class	25 µg/mL	50 µg/mL	100 µg/mL	200 µg/mL	400 µg/mL	600 µg/mL
0	41.3 ± 8.1	28.3 ± 2.1	23 ± 1	20 ± 2	20 ± 2	16 ± 1
1	21.6 ± 3	24.6 ± 0.57	25.3 ± 0.57	21.3 ± 2.3	23 ± 1	22.3 ± 2.5
2	16 ± 4.5	23.6 ± 1.5	19.6 ± 4.5	18.3 ± 3	19 ± 3	22.6 ± 2.5
3	11.6 ± 7.5	14 ± 3	19 ± 4	27.3 ± 1.5	20.6 ± 2.5	19 ± 4
4	9.3 ± 3.2	9.3 ± 2.5	13 ± 2	13 ± 2	17.3 ± 2.1	20 ± 3
TCS	126 ± 28	151.3 ± 2.3	173.6 ± 4.5	192 ± 1	194.3 ± 8	207.3 ± 2.5
H_2O_2						
Comet class	25 µg/mL	50 µg/mL	100 µg/mL	200 µg/mL	400 µg/mL	600 µg/mL
0	37 ± 7	24.6 ± 0.5	19 ± 4	15.6 ± 1.1	12.3 ± 0.5	10.3 ± 0.5
1	21 ± 3	23 ± 1	22.3 ± 1.5	17.6 ± 2.08	19.6 ± 0.5	15.3 ± 0.5
2	17.3 ± 2.5	24.3 ± 3.7	22.6 ± 4.04	20.6 ± 3.5	15 ± 1	19.6 ± 1.5
3	13 ± 7	15.3 ± 5.03	120 ± 5	26 ± 2	27 ± 2	33.3 ± 2.1
4	12 ± 2.1	12.6 ± 3	16 ± 5.5	20 ± 2	26 ± 2	21.3 ± 4.04
TCS	137.3 ± 19	168.3 ± 2.5	191.6 ± 9.4	217 ± 1	234.6 ± 2	240 ± 7.2

negative controls (untreated cells). For the assessment of comet tails, please refer to Figs. 7(a)–7(d). The TCS for all samples is also shown in Fig. 8.

Anticancer assay (cytotoxicity)

In the MTT assay, the AgNPs exhibited a higher apoptosis ability compared with the plant extract. Circular cells were reported at a toxic concentration of the sample and the pH of the media frequently became acidic, as estimated by comparison with the control, whereas at a nontoxic concentration, the cells resembled the control cells. The apoptotic morphological alterations of BHK-21 cells that were induced by AgNPs, doxorubicin (positive control),

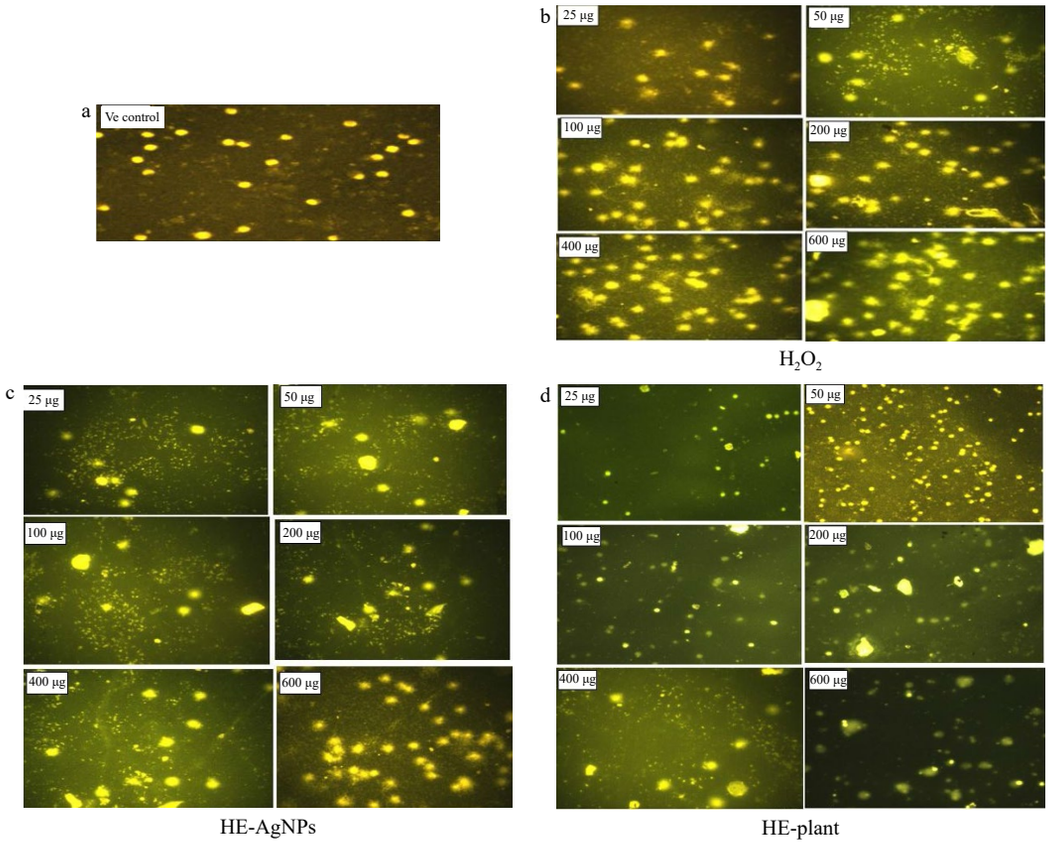

Fig. 7 Images of lymphocytes as comets. Comet images of **(a)** the negative control, **(b)** H_2O_2, **(c)** HE-AgNPs, and **(d)** the HE plant extract.

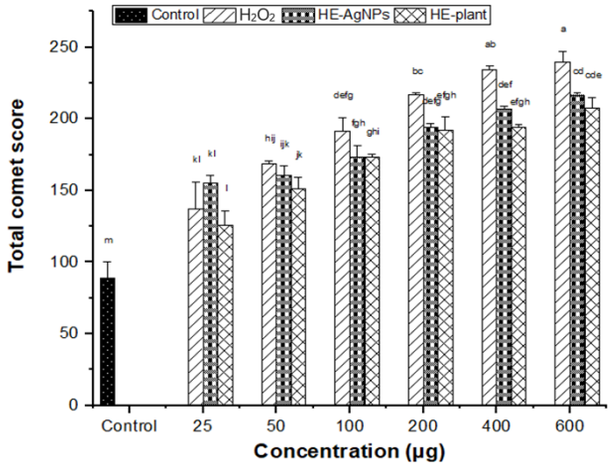

Fig. 8 Effect of the HE extract, HE-AgNPs, and H_2O_2 on the TCS in lymphocytes. The least significant difference (LSD) was 21.431; the data are reported in the form of averages and standard deviations. A two-way analysis of variance (ANOVA) with a threshold of significance of 5% was performed to compare the results ($P < 0.05$). The results indicated by similar letters were insignificant.

and the HE plant extract are shown in Figs. 9(a)–9(d). The negative control was blank (untreated cells). The morphological variation of the cells was screened using an inverted microscope. The current MTT dye assay showed that the HE-AgNPs exerted a significant cytotoxicity of 59% ± 0.8% at 600 µg/mL compared with the plant extract which (54% ± 0.7%), whereas AgNPs showed less cytotoxicity compared with doxorubicin (84.2%) at the same concentration of 600 µg/mL (Fig. 10).

IC_{50} determination

The concentrations of doxorubicin, HE-AgNPs, and HE extract that caused a 50% inhibition (IC_{50}) of BHK-21 cells were reported to be 134 ± 0.14, 421 ± 0.21, and 527 ± 0.23 µg, respectively. The IC_{50} was determined based on the percentage residual activity vs. the sample concentration (Figs. 11(a)–11(c)).

Discussion

The creation of NPs with remarkable optical and physical characteristics is the cornerstone of nanoscience. UV–Vis spectroscopy can be used to physically validate the synthesis of NPs in a solution of water [28]. Because of surface plasmon resonance, the color of NPs changes from milky to yellowish-brown. This conclusion is reinforced by [29].

A review of scientific studies revealed that FTIR is an excellent technique to identify functional group

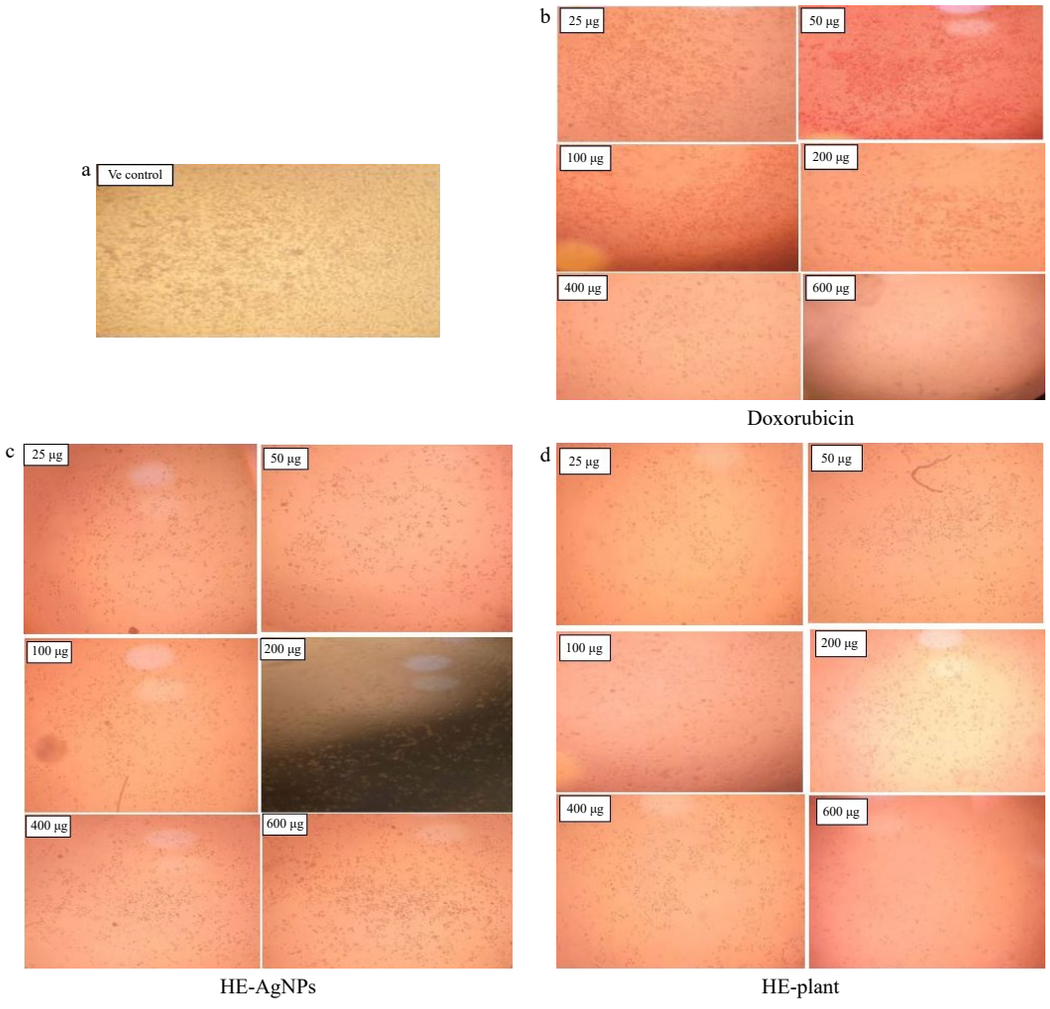

Fig. 9 Cancer cell imaging. **(a)** Untreated cells, **(b)** induced by HE extract, **(c)** induced by HE-AgNPs, and **(d)** induced by doxorubicin.

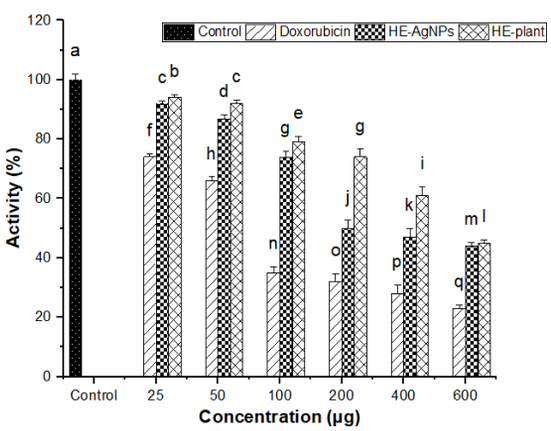

Fig. 10 Doxorubicin, the HE plant extract, and the AgNPs affected the viability of BHK-21 cells. The LSD was 0.165 6, and the data are presented as averages and standard deviations. To compare the results, a two-way analysis of variance (ANOVA) with a threshold of significance of 5% was used ($P < 0.05$). The results indicated by similar letters were insignificant. The experiment was repeated three times ($n = 3$).

subunits. Here, the FTIR examination indicated the presence of various functional groups, such as amino, hydroxyl, carbonyl, alkyne, alkene, alkane, amide, and carboxyl groups, which are involved in the reduction of the Ag ions to generate AgNPs persistently [30]. Surprisingly, these plant components played a crucial role in the stabilization of AgNPs, which is critical for their applicative qualities. These findings are consistent with reports from [31, 32].

The XRD examination of AgNPs revealed four unique peaks, confirming crystalline structure of the AgNPs. Similar findings have been reported by [6, 33]. The four distinct peaks obtained here were indicative of a face-centered cubic shape for AgNPs (ICDD PDF card number 00-004-0783) [34].

The topology and size of AgNPs were investigated using SEM, which revealed that the AgNPs had an irregular shape and were abundant. The SEM-determined size appeared to be larger than the XRD-calculated size, thus demonstrating the particle-agglomeration characteristics of the AgNPs. The previous report of [35] confirmed these findings; the

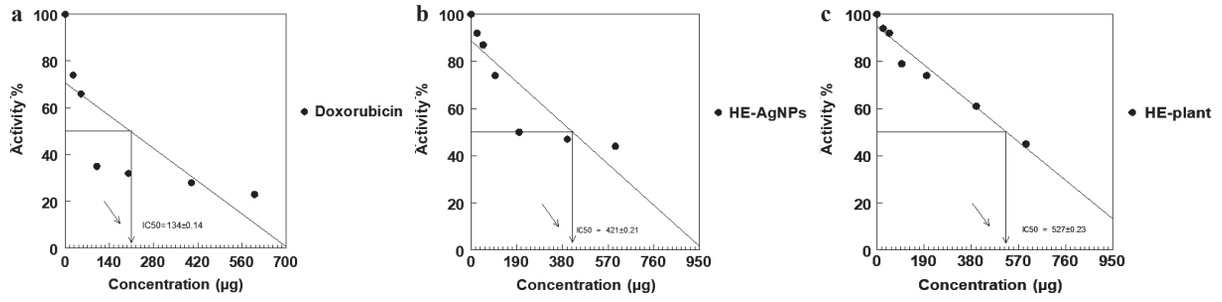

Fig. 11 IC_{50} values of **(a)** doxorubicin, **(b)** HE-AgNPs, and **(c)** HE plant extract.

difference in size observed between XRD and SEM was attributed to the agglomeration properties of AgNPs.

The EDX technique is employed for an elemental analyses [36, 37]. The Ag percentage in the AgNPs was determined to be significant in the current study, i.e., the AgNPs comprised 30.68% Ag, whereas the remaining constituents acted as covering organic compounds attached to the exterior of the AgNPs [38]. These results agree with those of Refs. [36, 39].

The biological manufacture and application of AgNPs has carved new possibilities for their use as anticancer and genotoxicity treatments. The use of NPs in nanotechnological clinical studies has recently grown into one of the most pressing topics in this field. The interaction between nanomaterials and live cells is unknown, as is their relationship with cellular and/or nuclear components. Therefore, it is critical to explore the potential cytotoxicity and genotoxicity of these nanomaterials, such as AgNPs. In the current work, even at very low dosages, AgNPs associated with BHK-21 cells and displayed *in vitro* cytotoxicity. AgNPs were less susceptible to the survival of BHK-21 cells and the cytotoxic effects of DNA damage than the HE extract. Cell death was demonstrated by the results of cytotoxicity assays. In our investigation, the cytotoxic effects of AgNPs with a length of 8.34 nm were more pronounced than those of the HE extract in decreasing cell viability. DNA damage to human blood cells was caused by AgNPs. The comet assay indicated that the DNA damage increased with increasing AgNP concentrations. Moreover, the AgNPs were found to be more harmful toward DNA compared with the plant extract. This DNA damage could point to a link between the size of AgNPs and their capacity to penetrate nuclear membranes and interact with DNA immediately. This greater cytotoxic effect for AgNPs, even at the same doses, could be attributed to their ability to penetrate cells. The findings of this investigation are consistent with those of Ref. [40], who proved that AgNPs that were as small as 1–40 nm were capable of entering cells with no harm. Furthermore, the authors of [41] reported that AgNPs with a dimension of 15 nm yielded comparable results. These findings are consistent with those of Ref. [42]. Smaller NPs penetrate through biological membranes more easily. They can also easily traverse the blood–brain barrier if their diameter is under 40 nm. Moreover, the NPs cause a dose-dependent increase in oxidation and DNA damage. NPs present in cells may accumulate in mitochondria, thus causing a reduction in the mitochondrial membrane potential, which interrupts ATP synthesis, and leads to ROS formation. Not only AgNPs themselves, but also the released Ag ions, generate ROS in cells. In turn, high ROS amounts lead to oxidative stress, which is responsible for the damage of cell membranes and the resulting damage to intracellular proteins, lipids, and DNA [43]. Higher ROS levels induce a cell response by activating proinflammatory signaling cascades and finally programmed cell death via either apoptosis or necrosis [44]. The carcinogenic and genotoxic consequences of NPs, such as AgNPs, were studied in Ref. [45]. Using the alkaline comet assay, the authors of Ref. [45] discovered that AgNPs produced DNA damage in human Mono Mac 6 cells and rat alveolar macrophages. Starch-induced NPs were tested on human glioblastoma (U251) and human lung fibroblast (IMR-90) cells, causing damage to DNA and cell-cycle arrest in the G2/M phase in a dose-dependent manner. This DNA damage was caused by the NP-driven disruption of the mitochondrial respiratory chain, which resulted in ROS production, the denaturation of enzymes, and the interruption of ATP production, leading to cellular homeostasis abnormalities and cell death [46, 47]. It is well recognized that the liver is the primary location of NP accumulation in humans. Regarding the utilization of NPs, the liver has been the subject of accelerated cancer research, as specific organs can be targeted if NPs are functionalized [48].

Conclusion

In conclusion, this investigation demonstrated the capacity of irregularly shaped AgNPs to reduce the viability of cells and cause damage to DNA in human blood lymphocytes, particularly when larger doses of AgNPs were used. The irregularly shaped AgNPs evaluated here exhibited higher cytotoxicity and genotoxicity compared with the HE extract. This study should be followed up to determine the ideal size and density of AgNPs that may be employed safely without harming normal cells.

CRediT Author Statement

Naila Sher: original draft writing. Mushtaq Ahmed: supervision. Nadia Mushtaq: data curation. Rahmat Ali Khan: methodology.

Conflict of Interest

The authors disclose they do not have a conflict of obligation.

References

[1] S.F. Sener, N. Grey. The global burden of cancer. *Journal of Surgical Oncology*, 2005, 92(1): 1−3. https://doi.org/10.1002/jso.20335

[2] C.D. Mathers, D. Loncar. Projections of global mortality and burden of disease from 2002 to 2030. *PLoS Medicine*, 2006, 3(11): e442. https://doi.org/10.1371/journal.pmed.0030442

[3] J.S. MacDonald. Toxicity of 5-fluorouracil. *Oncology*, 1999, 13(7 Suppl 3): 33–34.

[4] G. Rexroth, V. Scotland. Cardiac toxicity of 5-fluorouracil. *Med Klin* (*Munich*), 1994, 89(12): 680−688.

[5] N. Rastogi, M. Chag, S. Ayyagari. Myocardial ischemia after 5-fluorouracil chemotherapy. *International Journal of Cardiology*, 1993, 42(3): 285−287. https://doi.org/10.1016/0167-5273(93)90061-K

[6] N. Sher, M. Ahmed, N. Mushtaq, et al. *Calligonum polygonoides* reduced nanosilver: A new generation of nanoproduct for medical applications. *European Journal of Integrative Medicine*, 2020, 33: 101042. https://doi.org/10.1016/j.eujim.2019.101042

[7] N. Lewinski, V. Colvin, R. Drezek. Cytotoxicity of nanoparticles. *Small*, 2008, 4(1): 26−49. https://doi.org/10.1002/smll.200700595

[8] S. Kim, J.E. Choi, J. Choi, et al. Oxidative stress-dependent toxicity of silver nanoparticles in human hepatoma cells. *Toxicology in Vitro*, 2009, 23(6): 1076−1084. https://doi.org/10.1016/j.tiv.2009.06.001

[9] Y.P. Kwan, T. Saito, D. Ibrahim, et al. Evaluation of the cytotoxicity, cell-cycle arrest, and apoptotic induction byEuphorbia hirtain MCF-7 breast cancer cells. Pharmaceutical Biology, 2015: 1223–1235. https://doi.org/10.3109/13880209.2015.1064451

[10] M. Oves, M.A. Rauf, M. Aslam, et al. Green synthesis of silver nanoparticles by *Conocarpus Lancifolius* plant extract and their antimicrobial and anticancer activities. *Saudi Journal of Biological Sciences*, 2022, 29(1): 460−471. https://doi.org/10.1016/j.sjbs.2021.09.007

[11] Jannathul Firdhouse, M., Lalitha, P. Apoptotic efficacy of biogenic silver nanoparticles on human breast cancer MCF-7 cell lines. *Progress in Biomaterials*, 2015, 4: 113–121. https://doi.org/10.1007/s40204-015-0042-2

[12] S.R.K. Pandian, D. Anjanei, N.L. Raja, et al. PEGylated silver nanoparticles from Sesbania aegyptiaca exhibit immunomodulatory and anti-cancer activity. *Materials Research Express*, 2018, 6(3): 035402. https://doi.org/10.1088/2053-1591/aaf2d2

[13] S. Gurunathan, J.W. Han, A.A. Dayem, et al. Green synthesis of anisotropic silver nanoparticles and its potential cytotoxicity in human breast cancer cells (MCF-7). *Journal of Industrial and Engineering Chemistry*, 2013, 19(5): 1600−1605. https://doi.org/10.1016/j.jiec.2013.01.029

[14] N. Igaz, D. Kovács, Z. Rázga, et al. Modulating chromatin structure and DNA accessibility by deacetylase inhibition enhances the anti-cancer activity of silver nanoparticles. *Colloids and Surfaces B*: *Biointerfaces*, 2016, 146: 670−677. https://doi.org/10.1016/j.colsurfb.2016.07.004

[15] T.A.J. Souza, L.P. Franchi, L.R. Rosa, et al. Cytotoxicity and genotoxicity of silver nanoparticles of different sizes in CHO-K1 and CHO-XRS5 cell lines. *Genetic Toxicology and Environmental Mutagenesis*, 2016, 795: 70−83. https://doi.org/10.1016/j.mrgentox.2015.11.002

[16] X.M. Jiang, R. Foldbjerg, T. Miclaus, et al. Multi-platform genotoxicity analysis of silver nanoparticles in the model cell line CHO-K1. *Toxicology Letters*, 2013, 222(1): 55−63. https://doi.org/10.1016/j.toxlet.2013.07.011

[17] K.T. Rim, S.W. Song, H.Y. Kim. Oxidative DNA damage from nanoparticle exposure and its application to workers' health: A literature review. *Safety and Health at Work*, 2013, 4(4): 177−186. https://doi.org/10.1016/j.shaw.2013.07.006

[18] M. Ouedraogo, E. Camille Na, R. Semde, et al. *In vitro* biocompatibility and genotoxicity assessment of a gentamicin-loaded monoolein gel intended to treat of chronic osteomyelitis. *Journal of Pharmacology and Toxicology*, 2008, 3(5): 394–401. https://doi.org/10.3923/jpt.2008.394.401

[19] D. Philip, C. Unni, S.A. Aromal, et al. Murraya Koenigii leaf-assisted rapid green synthesis of silver and gold nanoparticles. *Spectrochimica Acta Part A*: *Molecular and Biomolecular Spectroscopy*, 2011, 78(2): 899−904. https://doi.org/10.1016/j.saa.2010.12.060

[20] K.R. Kirtikar, B.D. Basu. Indian Medicinal Plants : Vols. 1–4. 1991, Dehra Dun: Bishen Singh Mahendra Pal Singh.

[21] S. Ijaz, A. Perveen, N. Ghaffar. Preliminary phytochemical screening of seeds of Phytolacca latbenia (Moq.) walte. A wild medicinal plant of tropical and sub-tropical region of Pakistan. *Organic & Medicinal Chemistry International Journal*, 2019, 9(1): 555754. https://doi.org/10.19080/OMCIJ.2019.09.555754

[22] K.S. Prasad, N. Savithramma. Biosynthesis and validation of silver nanoparticles from Nymphaea caerulea *American Journal of Advanced Drug Delivery*, 2015, 3: 149–159.

[23] R. Geethalakshmi, DVL. Sarada. Characterization and antimicrobial activity of gold and silver nanoparticles synthesized using saponin isolated from *Trianthema decandr*a L. *Industrial Crops and Products*, 2013, 51: 107−115. https://doi.org/10.1016/j.indcrop.2013.08.055

[24] N. Sher, M. Ahmed, N. Mushtaq, et al. Cytotoxicity and genotoxicity of green synthesized silver, gold, and silver/gold bimetallic NPs on BHK-21 cells and human blood lymphocytes using MTT and comet assay. *Applied Organometallic Chemistry*, 2023, 37(2): e6968. https://doi.org/10.1002/aoc.6968

[25] A.R. Collins. The comet assay for DNA damage and repair: Principles, applications, and limitations. *Molecular Biotechnology*, 2004, 26: 249−261. https://doi.org/10.1385/mb:26:3:249

[26] M. Khisroon, A. Khan, M. Imran, et al. Biomonitoring of DNA damage in individuals exposed to brick kiln pollution from Peshawar Khyber Pakhtunkhwa, Pakistan. *Archives of Environmental & Occupational Health*, 2018, 73(2): 115−120. https://doi.org/10.1080/19338244.2017.1304881

[27] A. Balupillai, R.P. Nagarajan, K. Ramasamy, et al. Caffeic acid prevents UVB radiation induced photocarcinogenesis through regulation of PTEN signaling in human dermal fibroblasts and mouse skin. *Toxicology and Applied Pharmacology*, 2018, 352: 87−96. https://doi.org/10.1016/j.taap.2018.05.030

[28] N. Sher, M. Ahmed, N. Mushtaq. Synthesis, optimization, and characterization of silver/gold allied bimetallic from *Hippeastrum hybridum* (L.) and their ex vivo anti-acetylcholinesterase activity in rat brain. *Applied Organometallic Chemistry*, 2023, 37(5): e7082. https://doi.org/10.1002/aoc.7082

[29] K.B. Narayanan, N. Sakthivel. Biological synthesis of metal nanoparticles by microbes. *Advances in Colloid and Interface Science*, 2010, 156(1-2): 1−13. https://doi.org/10.1016/j.cis.2010.02.001

[30] P. Dauthal, Mukhopadhyay, M. Noble metal nanoparticles: Plant-mediated synthesis, mechanistic aspects of synthesis, and applications. *Industrial & Engineering Chemistry Research*, 2016, 55(36): 9557–9577. https://doi.org/10.1021/acs.iecr.6b00861

[31] B. Syed, N. Bisht, S.B. Prithvi, et al. Phytogenic synthesis of nanoparticles from *Rhizophora mangle* and their bactericidal potential with DNA damage activity. *Nano-Structures & Nano-Objects*, 2017, 10: 112−115. https://doi.org/10.1016/j.nanoso.2017.03.011

[32] Awwad, A. M., Salem, N. M., Abdeen, A. O. Green synthesis of silver nanoparticles using carob leaf extract and its antibacterial activity.*International Journal of Industrial Chemistry*, 2013, 4(1): 29. https://doi.org/10.1186/2228-5547-4-29

[33] H. Bar, D.K. Bhui, G.P. Sahoo, et al. Green synthesis of silver nanoparticles using seed extract of Jatropha curcas. *Colloids and Surfaces A*: *Physicochemical and Engineering Aspects*, 2009, 348(1-3): 212−216. https://doi.org/10.1016/j.colsurfa.2009.07.021

[34] L.K. Ruddaraju, P.N.V.K. Pallela, S.V.N. Pammi, et al. Synergetic antibacterial and anticarcinogenic effects of Annona squamosa leaf extract mediated silver nano particles. *Materials Science in Semiconductor Processing*, 2019, 100: 301−309. https://doi.org/10.1016/j.mssp.2019.05.007

[35] K. Kalimuthu, R. Suresh Babu, D. Venkataraman, et al. Biosynthesis of silver nanocrystals by *Bacillus licheniformis*. *Colloids and Surfaces B*: *Biointerfaces*, 2008, 65(1): 150–153. https://doi.org/10.1016/j.colsurfb.2008.02.018

[36] A.O. Dada, F.A. Adekola, E.O. Odebunmi. A novel zerovalent Manganese for removal of copper ions: Synthesis, characterization and adsorption studies. *Applied Water Science*, 2017, 7(3): 1409−1427. https://doi.org/10.1007/s13201-015-0360-5

[37] A.O. Dada, F.A. Adekola, E.O. Odebunmi. Kinetics and equilibrium models for sorption of Cu(II) onto a novel manganese nano-adsorbent. *Journal of Dispersion Science and Technology*, 2016, 37: 119−133. https://doi.org/10.1080/01932691.2015.1034361

[38] N. Sher, D.H.M. Alkhalifah, M. Ahmed, et al. Comparative study of antimicrobial activity of silver, gold, and silver/gold bimetallic nanoparticles synthesized by green approach. *Molecules*, 2022, 27(22): 7895. https://doi.org/10.3390/molecules2722789

[39] N. Sher, M. Ahmed, N. Mushtaq, et al. Enhancing antioxidant, antidiabetic, and antialzheimer performance of *Hippeastrum hybridum* (L.) using silver nanoparticles. *Applied Organometallic Chemistry*, 2022, 36(7): 6742. https://doi.org/10.1002/aoc.6724

[40] E. Connor, J. Mwamuka, A. Gole, et al. Gold nanoparticles are taken up by human cells but do not cause acute cytotoxicity. *Small*, 2005, 1(3): 325−327. https://doi.org/10.1002/smll.200400093

[41] M. Tsoli, H. Kuhn, W. Brandau, et al. Cellular uptake and toxicity of Au_{55} clusters. *Small*, 2005, 1(8-9): 841−844. https://doi.org/10.1002/smll.200500104

[42] N. Sher, M. Ahmed, N. Mushtaq, et al. Synthesis of biogenic silver nanoparticles from the extract of *Heliotropium eichwaldi* L. and their effect as antioxidant, antidiabetic, and anti-cholinesterase. *Applied Organometallic Chemistry*, 2023, 37(2): e6950. https://doi.org/10.1002/aoc.6950

[43] C.Z. Liao, Y.C. Li, S.C. Tjong. Bactericidal and cytotoxic properties of silver nanoparticles. *International Journal of Molecular Sciences*, 2019, 20(2): 449. https://doi.org/10.3390/ijms20020449

[44] M. Akter, M.T. Sikder, M.M. Rahman, et al. A systematic review on silver nanoparticles-induced cytotoxicity: Physicochemical properties and perspectives. *Journal of Advanced Research*, 2018, 9: 1−16. https://doi.org/10.1016/j.jare.2017.10.008

[45] J. Grigg, A. Tellabati, S. Rhead, et al. DNA damage of macrophages at an air-tissue interface induced by metal nanoparticles. *Nanotoxicology*, 2009, 3(4): 348−354. https://doi.org/10.3109/17435390903276917

[46] P.V. AshaRani, G. Low Kah Mun, M.P. Hande, et al. Cytotoxicity and genotoxicity of silver nanoparticles in human cells. *ACS Nano*, 2009, 3(2): 279−290. https://doi.org/10.1021/nn800596w

[47] R.S. Hamida, G. Albasher, M.M. Bin-Meferij. Oxidative stress and apoptotic responses elicited by nostoc-synthesized silver nanoparticles against different cancer cell lines. *Cancers*, 2020, 12(8): 2099. https://doi.org/10.3390/cancers12082099

[48] I.M.M. Paino, V.S. Marangoni, R. de Cássia Silva de Oliveira, et al. Cyto and genotoxicity of gold nanoparticles in human hepatocellular carcinoma and peripheral blood mononuclear cells. *Toxicology Letters*, 2012, 215(2): 119−125. https://doi.org/10.1016/j.toxlet.2012.09.025